Multiple magnetic states within the A phase determined by field-orientation dependence of Mn_{0.9}Fe_{0.1}Si

Peter E. Siegfried, Alexander C. Bornstein, Andrew C. Treglia, Thomas Wolf, and Minhyea Lee

Multiple magnetic states within the A-phase determined by field-orientation dependence of $\mathbf{Mn_{0.9}Fe_{0.1}Si}$

Peter E. Siegfried,[1] Alexander C. Bornstein[†],[1] Andrew C. Treglia,[1] Thomas Wolf,[2] and Minhyea Lee[1, *]

[1]*Department of Physics, University of Colorado, Boulder, CO 80309, USA*
[2]*Institute for Solid-State Physics, Karlsruhe Institute of Technology, D-76021 Karlsruhe, Karlsruhe, Germany*
(Dated: December 5, 2017)

We report three distinct regions within the A-phase in Fe-doped MnSi, based on the evolution of magnetoresistance and the Hall effect as a function of orientation of applied field. Fe impurities as pinning centers and crystalline anisotropy are found non-negligible only at the boundary of the A-phase. Electrical transport characteristics unique to the A-phase not only remain robust, but also indicate a freely rotating skyrmion lattice, decoupled from underlying crystal structure or impurity pinning.

PACS numbers:

Introduction Cubic B20 structured intermetallic magnets provide a rare opportunity to study unique properties of the non-trivial magnetic texture known as the magnetic skyrmion lattice (SkL) as a collection of particle-like individual skyrmions. A small pocket in the H-T phase diagram, where the SkL emerges is called the A-phase[1,2].

The similarities between SkL and vortex lattice phases in type-2 superconductors has been recognized and many efforts were devoted to exploring possible skyrmion states[3–5], analogous to those exhibited by superconducting vortices. In particular, the presence of quenched disorders in superconducting states have been known to drive the system into a variety of vortex states that exhibit unique electrical transport characteristics and a rich phase diagram[6]. While the role of quenched disorders in the SkL has been considered theoretically in a dynamic limit [7], the experimental examination is scarce. Quenched disorders are expected to cause deformation of the SkL arrangement[8] and to influence the strength of the emergent field and scattering rates of the conduction electrons. Therefore, tracking the electrical transport properties will shed light on the nature of the A-phase and possible discernible states within.

Within the A-phase, the conspicuous topological Hall effect is observed, which arises from the emergent gauge field $\mathbf{b}$ expressed as, $b_i = \frac{\Phi_0}{8\pi}\epsilon_{ijk}\hat{n}\cdot(\partial_j\hat{n}\times\partial_k\hat{n})$, where ϵ_{ijk} is the Levi-Civita symbol with the indices running over x, y, and z, $\hat{n}(\mathbf{r})$ is the unit vector of the magnetization $\mathbf{M}(\mathbf{r})$, and $\Phi_0 = h/|e|$[9–11]. The magnitude of this gauge field is estimated to as large as 20 – 45 T for Fe-doped MnSi, giving rise to a highly unusual H-profile of the Hall signal [8].

In this paper, we report the field angle dependence of the Hall signal, ρ_{yx} and magnetoresistance (MR) in the presence of quenched disorders viz. Fe-doping in MnSi. We focus on near and inside of the A-phase in the phase diagram to reveal discernible areas within the A-phase whose origin could be attributed to weak crystalline anisotropy and quenched disorders. We find that the A-phase is divided into three distinct regions, which we call Region I, II and III : Region I shows the most prominent crystalline anisotropy and pinning effects, yet overall, both turn out relatively weak. Region II corresponds to the center of the A-phase and is characterized by the angle-*independent* MR, occurring at the same magnitude of field, H_m at which the THE has a maximum magnitude at a given T. Region III is found at elevated T and H above Region II, where the $\rho_{yx}(H)$ remains constant with increasing H and both MR and Hall signals as a function of the field angle recover the usual functional forms, indicating the background magnetization smoothly increases to the full spin-polarized state.

Methods Single crystals of $\mathrm{Mn_{0.9}Fe_{0.1}Si}$ (T_C = 6.9 K) used were grown by the Bridgman technique and cut into rectangular prisms for a standard 6-contacts geometry. Samples were mounted on a home-built rotation probe which allows full 2π rotation of the applied magnetic field in the xz-plane with the current $\mathbf{I} \parallel \hat{y}$, as shown in Fig. 2(a). Polar angle θ is measured from the $\hat{z}$ axis parallel to the crystallographic axis $\langle 111 \rangle$. Longitudinal (ρ) and Hall resistivity (ρ_{yx}) presented here are symmetrized and antisymmetrized, respectively, with respect to the polarity of H and θ. We found the demagnetization correction is negligible compared to magnitudes of features reported here (see Supplementary Materials[12]).

Results Unlike epitaxially grown films of MnSi or $\mathrm{Mn_{1-x}Fe_xSi}$[13,14], the THE signal can be easily identified from the unique H-profile in bulk crystalline samples. Fig. 1(a) shows the progression of $\rho_{yx}(H)$ in the A-phase (the shaded area). At $T = 5.50$ K, $\rho_{yx}(H)$ displays the onset of the THE, persisting throughout the range of T of the shaded region and the narrow bounds of the applied field. As T increases, the small bump in the H-profile, starting at around $H \simeq 0.3$ T at as low as $T = 5.25$ K, develops into a "peak-like" anomaly and then "shoulder-like", where $\rho_{yx}(H)$ remains constant until merging to the background. This region of T and H is referred to as the A-phase. We note the signs of the anomalous Hall signal and THE of $\mathrm{Mn_{0.9}Fe_{0.1}Si}$ here are found to be opposite from those of pure MnSi, attributed to sufficiently large Fe doping that alters the electronics structure responsible for the sign of the Berry phase contribution and
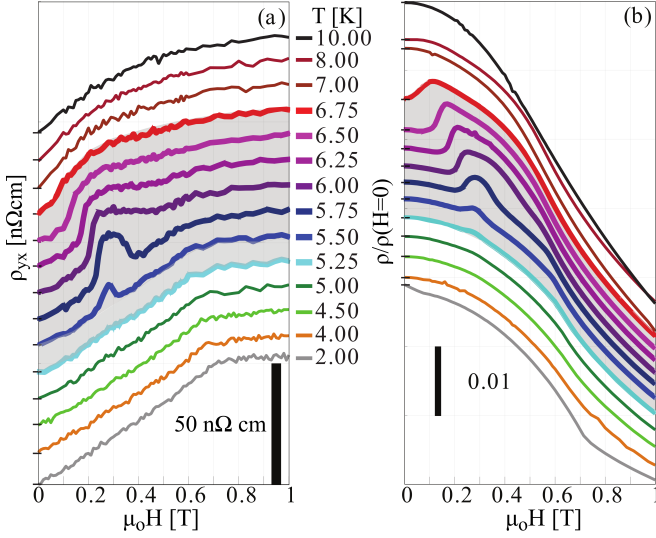
FIG. 1: (a) Hall resistivity $\rho_{yx}(H)$ and (b) fMR $\rho(H)/\rho(H = 0)$ as a function of H are plotted with offset for clarity. Gray shaded areas indicates the T-ranges corresponding to the A-phase (thick lines).

FIG. 2: (a)(Left) Measurement configuration with a bar-shaped $Mn_{0.9}Fe_{0.1}Si$. θ measured from the $\langle 111 \rangle$ direction sweeps through $\langle 010 \rangle$. (Right) Image of $Mn_{0.9}Fe_{0.1}Si$ crystal with crystallographic faces labeled via X-ray single crystal diffraction. (b) Normalized Hall resistivity $\rho_{yx}(\theta)/\rho_{yx}^0$ at fixed $H = 0.15$ (red), 0.175 (green) and 1 T (light blue) at $T = 4.5$ K and (c) at 6 K. (d) θ dependence of normalized MR at $T = 4.5$ K and (e) at 6 K. Broken lines establish $\cos\theta$ and $\cos 2\theta$ for Hall and MR respectively.

the polarity of the effective carrier[8].

Similar progression of the H dependence is also found in fractional MR (fMR), defined as $\frac{\rho(H)}{\rho(H=0)}$, shown in Fig. 1(b) in the shaded area. Entering the A-phase with increasing H, MR becomes enhanced due to the increased spin scattering arising from the SkL texture simultaneously to the emergence of the THE signal. This enhancement collapses back as exiting the A-phase, resulting in the peak-like feature in MR as well. At higher T's (6.00 and 6.25 K), MR undergoes similar changes to the Hall signal, exhibiting the shoulder-like H-dependence when approaching the spin polarization field (H_P). Beyond H_P, it decreases rapidly due to the significantly reduced spin scattering in the polarized state. .

We first establish the baseline of the field orientation dependence outside of the A-phase, where the MR and Hall signals unequivocally exhibit $\cos 2\theta$ and $\cos\theta$ dependences, respectively. Fig. 2 (b, c) displays the angular dependence of the normalized Hall resistivity, $\rho_{yx}(\theta)/\rho_{yx}^0$, where $\rho_{yx}^0 = \rho_{yx}(\theta = 0)$ at the given H's and T's of which values lie well outside of the A-phase. Since ρ_{yx} in this region is largely contributed from anomalous Hall effect due to the background magnetization (M) the $\cos\theta$ dependence indicates smooth rotation of M along H. Fig. 2 (d,e) displays the angle dependence of normalized MR, $\rho(\theta)/\rho^0$, where $\rho^0 = \rho(\theta = 0)$. Two MR curves track the $\cos 2\theta$ dependence, which is expected for soft ferromagnetic metals, known as anisotropic magnetoresistance[15]. Note that the angle sweep at $H = 0.15$ T at 4.5 K shows a distinct curvature near $\theta = 0$, which clearly differs from that of 6 K. This is supposed to arise from the depinning of the helical propagation direction[5].
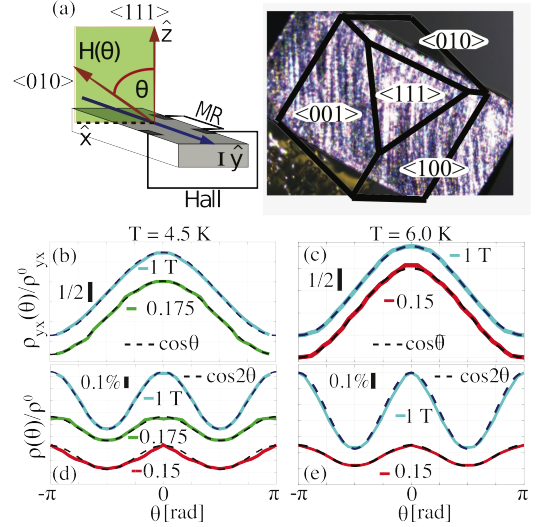
Next, we present the results on angular dependences of

ρ_{yx} and MR at three representative T's – 5.50, 5.75 and 6.26 K – within the A-phase. Fig. 3(a-d) shows $\rho_{yx}(H)$ [(a)], fMR (H) [(c)] and θ-dependences of the normalized resistivities $\rho_{yx}(\theta)/\rho_{yx}^0$ [(b)] and $\rho_{yx}(\theta)/\rho_{yx}^0$ [(d)] at $T = 5.50$ K, where both the THE and enhanced MR begin to emerge. In the H range of $0.175 < \mu_0 H < 0.250$ T, the angle dependences exhibit strong deviations from the cosine functions, shaded in (b) and (d). Weak THE signal indicates either low density and/or an imperfect lattice of skyrmions. Similarly, deviations from $\cos 2\theta$ observed in MR [Fig. 3(d)] point to the onset of the A-phase.

Fig. 3(e-h) shows the set of data at $T = 5.75$ K. Here, both Hall and MR angle data start with following usual $\cos\theta$ and $\cos 2\theta$ at low field [green curves in (f) and (h)]. Then, MR signal consequently go through two H-region of strong deviation from $\cos 2\theta$ function [red shade in (h)], which are separated by the striking θ-independent MR [thick lines in yellow shade]. Meanwhile, the Hall data also shows the deviations from $\cos\theta$ in two red shaded regions but it recovers the strict $\cos\theta$ form in the yellow region. Further increasing H, exiting the A-phase and entering the conically-ordered state, the cosine function dependences are recovered.

We note that the narrow field range of the isotropic MR in the yellow shade (i.e. $\rho(\theta)/\rho^0$ remains constant) include the H_m [Fig. 3(e)], indicating the SkL lattice is fully formed and the magnitude of the resulting gauge field is at its largest. The simultaneous recovery of $\cos\theta$ in Hall evidences that the SkL plane rotates freely along
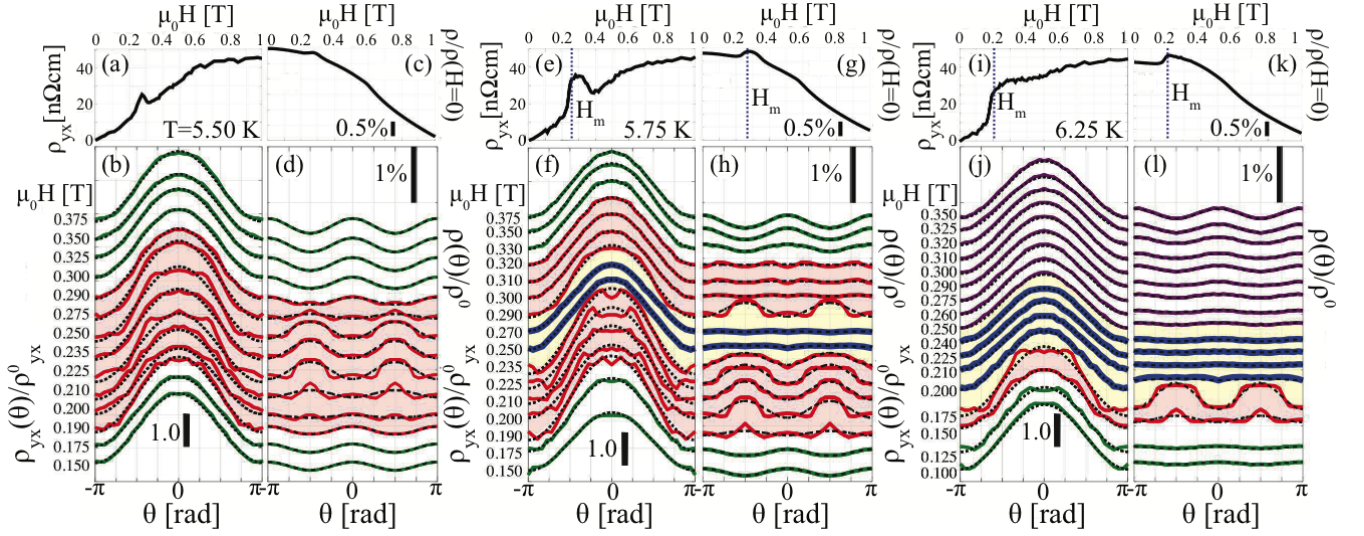
FIG. 3: (a-d) $\rho_{yx}(H)$, $\rho_{yx}(\theta)/\rho_{yx}^0$, $\rho(H)/\rho(H=0)$ and $\rho(\theta)/\rho^0$ at $T = 5.50$ K, (e-h) $T = 5.75$ K, (i-j) $T = 6.25$ K. Note both (h) and (l) show the angle-independent region that separates two different θ-dependence. The angle sweep curves are shown with offsets for clarity. The regions outside of the A-phase are plotted in green. Region I, II and III are marked with red, yellow, and purple shading respectively. Broken black lines show $\cos\theta$ and $\cos 2\theta$ dependences for Hall and MR, respectively.

the applied field direction, decoupled from the lattice or pinning centers. This makes it plausible to have a constant spin-scattering rate that leads to constant MR upon rotating the orientation of H.

Fig. 3(i-l) shows the same set for $T = 6.25$ K. Here, $\rho_{yx}(\theta)/\rho^0$ shows a clear deviation from $\cos\theta$ only in the low H [red shade in (j)] but it remains in the $\cos\theta$ form for the rest of the H's. On the other hand, MR exhibits the same θ-independent region [yellow shade in (l)] followed by the strong deviation from $\cos 2\theta$ form [red shade]. In high H, it smoothly transforms to $\cos 2\theta$ form, which is different from what was observed at lower T [Fig. 3(f) and (h)].

Based on these observations, we classify the A-phase and the immediate surroundings into three separate regions in the H-T phase diagram:

(1) Region I : Red-shaded regions [Fig. 3(b,d,f,h) and (j,l)] are marked by the deviations from $\cos\theta$ (Hall) and $\cos 2\theta$ (MR) dependence. The irregular θ-dependence in this region is ascribed to crystallogrphic orientation dependence or pinning of skyrmions during the nucleation and annihilation of individual skyrmions or the SkL. In low T of this region [Fig. 3(b,d)], the SkL is still premature so that the resulting gauge field responsible for THE must be weak. Thus nucleation of skyrmions and the SkL encounter pinning from the impurities and the crystalline anisotropy[16–18], preventing it from closely following the applied field direction resulting in strong deviations from $\cos\theta$ dependence. At higher T, this region occurs at at nucleation (lower H) and annihilation (higher H), from which we deduce that the effect of crystalline anisotropy and pinning effect is most prominent as entering and exiting the A-phase.

(2) Region II : Yellow-shaded regions [Fig. 3(f,h) and (j,l)] are marked by the constant MR upon rotating H, indicating the emergence of the fully developed SkL decoupled completely from the crystalline lattice and pinning sites. Here the Hall signal reaches its maximum, simultaneously recovering $\cos\theta$ dependence, from which we infer that the SkL is fully formed and generating the maximum magnitude of the gauge field. This region occupies a narrow range of H at the center of the A phase, although it extends close to T_C.

(3) Region III : Purple-shaded region [Fig. 3(j,l)] is marked by the smooth recovery $\cos 2\theta$ after θ-independent MR. We note, in this region, the H dependences of THE and MR exhibit "shoulder-like" features, where the magnetic state in the H range of constant MR and Hall should be discernible from the conical state. Approaching T_C near the upper T and H boundary of the A-phase, the SkL maintains the long range translational symmetry while the individual skyrmions are polarized and thus, the emergent field is reduced to to zero smoothly. This results in $\cos 2\theta$ dependence being recovered in the MR, with no sign of exiting the A-phase (i.e. without having Region I in the high H). It is consistent with the shoulder-like H-dependence in ρ_{yx}.

The resulting phase diagram is presented in Fig. 4, where Region I, II and III are indicated. The colormap is generated from $\Delta\rho_{yx}(H)$, obtained by subtracting the T-dependent linear background up to $H = H_p$ from $\rho_{yx}(H)$ [Fig. 1(a)]. The overlaid symbols correspond to the values of (T, H) of $\rho(\theta)/\rho^0$ (white triangle) and $\rho_{yx}(\theta)/\rho_{yx}^0$ (black square), from the different angle dependences in the Hall and MR data. These clearly illustrate the three different regions of the A-phase discussed above. We ex-
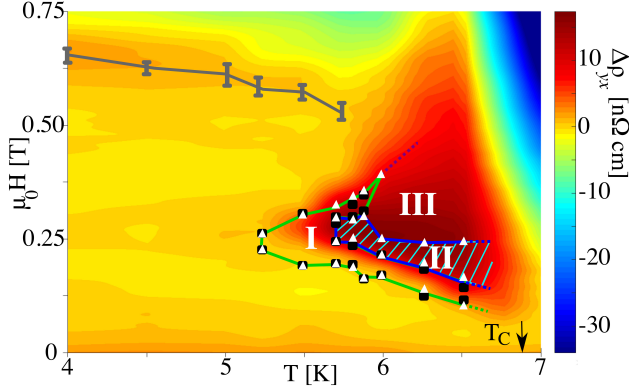
FIG. 4: Color map generated from $\Delta\rho_{yx}$, calculated by subtracting the linear background below spin polarization field $\rho_{yx}(H)$. The gray line refers to the onset of spin-polarization marked from the kink in $\rho_{yx}(H)$ shown in Fig. 1(a). Three distinct Regions I, II and III are explicitly identified by the field orientation and magnitude dependence (See text).

amined a different Fe doping (8%) sample and found the angle and field dependence are consistent [12]. This supports our conclusion that these three regions are not specific to a particular Fe contents but can be a general trait for the A-phase.

Discussion It is intriguing to juxtapose our classification of the A-phase to what was found in the LTEM images in pure MnSi crystals: Multi-domain SkL, single-domain SkL and skyrmion glass[19]. The multi-domain SkL consists of separate hexagonal skyrmion lattices existing with distinct boundaries between different orientations similar to grain boundaries of polycrystalline materials. In the LTEM observation in Ref.[19], this state appears at low H area of the A-phase, similar to our Region I. The multi-domain SkL implies long range translational symmetry has not been fully established yet. The domain boundary is likely to form along the impurities, in analogy to the superconducting vortex. Deformation from the regular triangular lattice would result in a weaker THE signal, yet still yield the peak-like H profile. The increased spin scattering due to the nucleating skyrmions also leads to the increase in MR in this narrow range of field.

On the other hand, the fully formed single-domain SkL phase of Region II generates the largest and most robust magnitude of the THE, while it is oblivious to the presence of disorder, and the planes of the SkL, and thus the orientation of the gauge field, closely follow the direction of H.

The state in further increased H is denoted as the skyrmion glass phase [19]. Here the individual skyrmions are inferred to be in the process of being polarized, as if dissolving into the ferromagnetic state, while the triangular SkL is still maintained. This corresponds to Region III, where the spins comprising the SkL are diffused by applied H, yet the periodic structure of the SkL maintains a non-zero gauge field. It seems that the transition from single domain SkL to skyrmion glass is smooth and adiabatic. Such change is known to have little effect on the THE[20], which is consistent with $\cos\theta$ dependence of ρ_{yx} in our data.

Overall, we find the role of impurities as pinning centers is feeble and ineffective. In fact, there is no clear argument nor evidence to distinguish the effects originated from of weak crystalline anisotropy and originated from pinning centers, as both would leave distinct non-trivial angular dependences within the A-phase in the electrical transport data. This is consistent with the theoretical consideration that strong interaction with impurity sites occurs at the time of nucleation[21]. From the way Region I surrounds Region II [Fig. 4] we deduce that in Region I, the nucleation of the skyrmions and the SkL is the most receptive to the crystalline anisotropy and the presence of quenched disorders.

Region II resembles the previously reported A-phase core[5] in pure MnSi in terms of constant $\rho(\theta)$ upon rotating field. However, robust $\cos\theta$ dependence indicates that the emergent field freely rotates along with the applied field, independent from underlying crystallinity and pinnings. In the comparison with pure MnSi, the size of the magnetic moment is reduced by a factor of two and T_C by a factor of four. Also, the residual resistivity increases 20 times in $Mn_{0.9}Fe_{0.1}Si$ which leaves the mean free path of electron only up to a few percent of the lateral size of the SkL[8,22]. Despite these effects, the remarkable robustness found in electrical transport properties in the A-phase is expected to play an essential role in developing skyrmion-based devices and hosting materials and is particularly noticeable in Region II and III.

Summary We identify three distinct regions within the A-phase in $Mn_{0.9}Fe_{0.1}Si$, reflecting a series of distinct SkL states from nucleating out of conical ordering to vanishing into spin polarized state as a function of T and H. The roles of crystalline anisotropy and pinning due to Fe impurities is only discernible in Region I. Experimental distinction of the multiple magnetic states provides the basis for flexible geometries in devices utilizing skyrmion-based electrical responses. We looked for possible signatures that distinguish Region I and II in magnetization measurements for a few different angles but found such features are within the noise-level and far from conclusive[12]. Further investigation will definitely be beneficial to understanding the nature of these states.

[†]Current Address: Department of Applied Physics, Stanford University, Palo Alto CA

[*] Electronic address: minhyea.lee@colorado.edu

[1] C. Thessieu, C. Pfleiderer, A. N. Stepanov, and J. Flouquet, J. Phys.: Condens. Matter **9**, 6677 (1997).

[2] S. Muhlbauer, B. Binz, F. Jonietz, C. Pfleiderer, A. Rosch, A. Neubauer, R. Georgii, and P. Boni, Science **323**, 915 (2009).

[3] H. Wilhelm, M. Baenitz, M. Schmidt, U. K. Rößler, A. A. Leonov, and A. N. Bogdanov, Phys. Rev. Lett. **107**, 127203 (2011), URL http://link.aps.org/doi/10.1103/PhysRevLett.107.127203.

[4] O. Janson, I. Rousochatzakis, A. A. Tsirlin, M. Belesi, A. A. Leonov, U. K. Rössler, J. van den Brink, and H. Rosner, Nature communications **5**, 5376 (2014).

[5] I. Lobanova, V. Glushkov, N. Sluchanko, and S. Demishev, Scientific reports **6** (2016).

[6] G. Blatter, M. V. Feigel'man, V. B. Geshkenbein, A. I. Larkin, and V. M. Vinokur, Rev. Mod. Phys. **66**, 1125 (1994), URL http://link.aps.org/doi/10.1103/RevModPhys.66.1125.

[7] C. Reichhardt, D. Ray, and C. J. O. Reichhardt, Phys. Rev. Lett. **114**, 217202 (2015), URL http://link.aps.org/doi/10.1103/PhysRevLett.114.217202.

[8] B. J. Chapman, M. G. Grossnickle, T. Wolf, and M. Lee, Physical Review B **88**, 214406 (2013).

[9] A. N. Bogdanov and D. A. Yablonskii, Sov. Phys. JETP **68**, 101 (1989).

[10] U. Rößler, A. Bogdanov, and C. Pfleiderer, Nature **442**, 797 (2006).

[11] T. Schulz, R. Ritz, A. Bauer, M. Halder, M. Wagner, C. Franz, C. Pfleiderer, K. Everschor, M. Garst, and A. Rosch, Nature Physics **8**, 301 (2012).

[12] See the Supplementary Materials.

[13] Y. Li, N. Kanazawa, X. Yu, A. Tsukazaki, M. Kawasaki, M. Ichikawa, X. Jin, F. Kagawa, and Y. Tokura, Physical review letters **110**, 117202 (2013).

[14] T. Yokouchi, N. Kanazawa, A. Tsukazaki, Y. Kozuka, M. Kawasaki, M. Ichikawa, F. Kagawa, and Y. Tokura, Physical Review B **89**, 064416 (2014).

[15] T. McGuire and R. Potter, IEEE Trans. Magn. **11**, 1018 (1975).

[16] A. Neubauer, C. Pfleiderer, B. Binz, A. Rosch, R. Ritz, P. G. Niklowitz, and P. Böni, Phys. Rev. Lett. **102**, 186602 (2009), URL http://link.aps.org/doi/10.1103/PhysRevLett.102.186602.

[17] A. Bauer, A. Neubauer, C. Franz, W. Münzer, M. Garst, and C. Pfleiderer, Phys. Rev. B **82**, 064404 (2010), URL http://link.aps.org/doi/10.1103/PhysRevB.82.064404.

[18] A. Bauer and C. Pfleiderer, Phys. Rev. B **85**, 214418 (2012), URL http://link.aps.org/doi/10.1103/PhysRevB.85.214418.

[19] X. Yu, A. Kikkawa, D. Morikawa, K. Shibata, Y. Tokunaga, Y. Taguchi, and Y. Tokura, Physical Review B **91**, 054411 (2015).

[20] M. B. Jalil and S. G. Tan, Scientific reports **4**, 5123 (2014).

[21] H. C. Choi, S.-Z. Lin, and J.-X. Zhu, Phys. Rev. B **93**, 115112 (2016), URL http://link.aps.org/doi/10.1103/PhysRevB.93.115112.

[22] S. V. Grigoriev, V. A. Dyadkin, E. V. Moskvin, D. Lamago, T. Wolf, H. Eckerlebe, and S. V. Maleyev, Phys. Rev. B **79**, 144417 (2009), URL http://link.aps.org/doi/10.1103/PhysRevB.79.144417.